

PROCEEDINGS

Open Access

# How does heparin prevent the pH inactivation of cathepsin B? Allosteric mechanism elucidated by docking and molecular dynamics

Mauricio GS Costa<sup>1\*</sup>, Paulo R Batista<sup>1</sup>, Cláudio S Shida<sup>1,2</sup>, Charles H Robert<sup>3</sup>, Paulo M Bisch<sup>1</sup>, Pedro G Pascutti<sup>1</sup>

From 5th International Conference of the Brazilian Association for Bioinformatics and Computational Biology (X-meeting 2009)

Angra Dos Reis, RJ, Brazil. 18-22 October 2009

## Abstract

**Background:** Cathepsin B (catB) is a promising target for anti-cancer drug design due to its implication in several steps of tumorigenesis. catB activity and inhibition are pH-dependent, making it difficult to identify efficient inhibitor candidates for clinical trials. In addition it is known that heparin binding stabilizes the enzyme in alkaline conditions. However, the molecular mechanism of stabilization is not well understood, indicating the need for more detailed structural and dynamic studies in order to clarify the influence of pH and heparin binding on catB stability.

**Results:** Our pKa calculations of catB titratable residues revealed distinct protonation states under different pH conditions for six key residues, of which four lie in the crucial interdomain interface. This implies changes in the overall charge distribution at the catB surface, as revealed by calculation of the electrostatic potential. We identified two basic surface regions as possible heparin binding sites, which were confirmed by docking calculations. Molecular dynamics (MD) of both *apo* catB and catB-heparin complexes were performed using protonation states for catB residues corresponding to the relevant acidic or alkaline conditions. The MD of *apo* catB at pH 5.5 was very stable, and presented the highest number and occupancy of hydrogen bonds within the inter-domain interface. In contrast, under alkaline conditions the enzyme's overall flexibility was increased: interactions between active site residues were lost, helical content decreased, and domain separation was observed as well as high-amplitude motions of the occluding loop – a main target of drug design studies. Essential dynamics analysis revealed that heparin binding modulates large amplitude motions promoting rearrangement of contacts between catB domains, thus favoring the maintenance of helical content as well as active site stability.

**Conclusions:** The results of our study contribute to unraveling the molecular events involved in catB inactivation in alkaline pH, highlighting the fact that protonation changes of few residues can alter the overall dynamics of an enzyme. Moreover, we propose an allosteric role for heparin in the regulation of catB stability in such a manner that the restriction of enzyme flexibility would allow the establishment of stronger contacts and thus the maintenance of overall structure.

\* Correspondence: maucosta@biof.ufjf.br

<sup>1</sup>Instituto de Biofísica Carlos Chagas Filho, Universidade Federal do Rio de Janeiro, 21949-901, Rio de Janeiro, Brasil

Full list of author information is available at the end of the article

## Background

Cathepsin B (EC 3.4.22.1) (catB) is one of the most well-characterized cysteine proteases, belonging to the clan CA (papain superfamily). In humans, its physiological role is implicated in bone resorption, antigen processing and protein turnover [1]. However, catB also participates in pathological processes such as cardiovascular disturbances [2], parasitic infections [3], Alzheimer's disease [4], osteoarthritis [5], tumor invasion and metastasis development [6,7]. Its main roles in cancer are *i*) its activity in directly cleaving extracellular matrix (ECM) components, *ii*) its activation of other ECM degrading proteases, which promotes tumor cell invasion into the surrounding tissue and bloodstream escape [8], and *iii*) stimulating angiogenesis which provides increased nutrients and oxygen supplies to cancer cells [9]. Thus, catB regulates several crucial steps in tumorigenesis and is a promising target for anti-cancer drug design [10].

Structurally, catB possesses the regular fold of papain-like enzymes, enclosing two distinct domains stabilized by six disulfide bridges, forming a large polar interface into which project the side chains of a few charged residues such as E171 and E36 (see Fig. 1). This interdomain interface is extremely important to catB overall activity as it comprises the active site residues (C29, H199 and N219). Unlike other members of the papain family, catB exhibits both exo- and endo-proteolytic

activities. Its exo-activity is dependent on the presence of two adjacent histidine residues (H110 and H111) located at an insertion region called the "occluding loop". These residues provide the necessary positive charge to anchor the negatively-charged C-terminal carboxylate of exo-substrates [11,12]. This region is only found in catB within its family, and it controls the access of large substrates to the active site [12]. Site-directed mutagenesis studies confirmed the role of the occluding loop since deletion of this entire region impairs exo- but not endo-proteolytic activity [13]. Additionally, this region confers thermal stability to catB and resistance against endogenous inhibitors such as cystatin C [13,14].

Currently the most potent and selective structure-based designed compounds available are derived from E-64 targeting the unusual occluding loop present in the catB 3D-structure [15]. However, enzymatic assays have shown that these inhibitors are strongly pH dependent as their optimal binding affinities are considerably diminished under neutral/alkaline conditions [16]. Since catB can be found in several cellular compartments with distinct pH values, these inhibitors are not effective *in vivo*. When catB is within the lysosomal or endosomal vesicles it confronts acidic conditions, in contrast to the neutral/alkaline environment when it is attached to membranes (mainly in caveolar microdomains) [17,18]

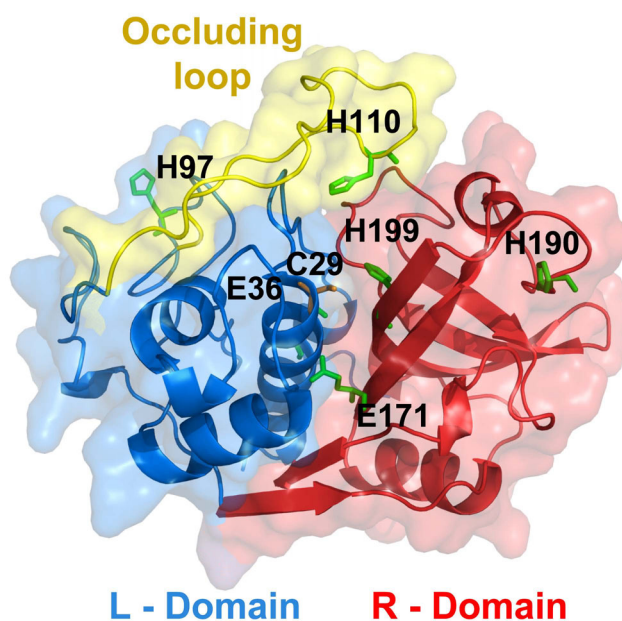


**Figure 1** Localization of differentially protonated residues in catB. Cartoon representation of the catB tertiary structure showing differentially protonated residues as green sticks. Protonation states were assigned to represent acidic (pH 5.5) or alkaline conditions (pH 8) based on pKa calculations with PROPKA on the catB crystal structure. The L and R domains of the protein are highlighted blue and red, respectively. The occluding loop (residues 106-124) a structural element found only in catB within its family, is represented in yellow.

or secreted in the ECM [19]. Although catB is rapidly inactivated under alkaline pH conditions, it was reported that membrane-associated forms are resistant to this process [20]. This peculiarity is believed to occur due to its interaction with heparan sulfate glycosaminoglycans (GAGs) on the cell surface [19]. This polysaccharide, structurally related to heparin, acts on the ECM as a co-receptor for several molecules such as growth factors and proteases [21]. Interaction between catB and heparin-like GAGs was already shown to prevent the enzyme's inactivation in high pH [22]. The main reported outcome was the maintenance of catB helical content in the presence of heparin at high pH, which was observed for papain as well [22,23]. Nevertheless, it has not been possible to precisely define the catB/heparin interaction sites and the molecular mechanism responsible for this protective effect.

Structural and molecular modelling studies can give insight into the molecular events concerning the modification of catB activity by pH changes and heparin binding. Some attempts have already been made towards designing new catB inhibitors using molecular modeling techniques [24,25], taking into account dynamical aspects of binding. However, these studies did not evaluate the influence of pH nor that of heparin binding on the modulation of the enzyme intrinsic flexibility.

In order to understand the heparin protective effect over catB structure we performed molecular dynamics (MD) simulations using an approach in which different pH conditions were taken into account by considering different protonation states of titratable groups on the protein surface. Further, docking analyses resulted in the identification of two heparin binding sites on catB structure. The MD calculations confirmed an increase of the overall catB flexibility and the loss of stability of the *apo* catB inter-domain interface in alkaline pH. The destabilization and the increased flexibility, notably in the occluding loop, were prevented by interaction with heparin, again in agreement with experimental data. We observed a role of active site residues in enzyme stabilization and in maintaining the helical content, and we propose an allosteric mechanism for the stabilizing effect promoted by GAG interaction. Taken together, our data provides an improved understanding of the molecular mechanisms responsible for both pH-induced inactivation and protection against inactivation by heparin binding.

## Results and discussion

### pH changes result in distinct protonation profiles

Prediction of pKa's for protein ionizable residues is an important tool for understanding features and catalytic mechanisms of pH-dependent enzymes [26]. We applied the PROPKA program to estimate pKa values in the

catB structure and to determine the most probable corresponding protonation states of the enzyme under acidic and alkaline conditions. Two different conditions were studied: acidic (pH 5.5), and alkaline (pH 8.0), which allow comparison to available experimental data [22].

It is known that catalytic residues often present unusual pKa values compared to those of free amino acids in solution [27]. Accordingly, our results for catB predicted a pKa of 2.14 for the catalytic C29, in contrast to 8.0 expected in solution. Previous work on the papain catalytic cysteine (structurally related to C29 in catB) showed pKa values around 2.5 to 3.5 [28], in accordance to our estimation for C29.

Comparing the acidic and alkaline conditions we observed that six key residues are differentially protonated. Table 1 gives the pKa values for these residues and Fig. 1 shows their positions in the catB structure. We note that four of these residues belong to the inter-domain interface (E36, H199, E171 and H110). The predicted pKa for E171 is 7.71, as carboxyl groups usually exhibit high pKa values in buried hydrophobic environments [26]. From our prediction we observed that both E171 and E36 are likely to be protonated at pH 5.5 but not in alkaline conditions.

As expected, most of the residues with differing protonation states were histidines, with a pKa in solution of 6.5 and an ionization state that is very susceptible to pH changes in the physiological range. H110 is a key residue for stabilization of the occluding loop and is also crucial for the exo-proteolytic activity of catB, since along with H111 it anchors the carboxyl terminus of substrates. Interestingly, we observed an pKa of 7.79 for the catalytic H199, which implies that this residue is protonated only in acidic conditions. This result is correspondent to the measured pKa of H159 in papain [28]. In papain, it was previously reported that the

**Table 1 Differentially protonated residues in catB and pKa values**

Residue	predicted crystal	Average values during 40ns MD	
		pH 5,5	pH 8
<b>C29</b>	2,14	3.7 ± 1.5	<b>7.3 +1.6</b>
<b>E36</b>	5,9	5.4 ± 0.5	3.4 ± 1.2
<b>H97</b>	6,9	7.1 ± 0.2	7.3 ± 0.4
<b>H110</b>	6,6	6.6 ± 0.8	8.1 ± 0.7
<b>E171</b>	7,7	7.4 ± 0.2	6.5 ± 0.4
<b>H190</b>	7,2	7.1 ± 0.2	7.4 ± 0.7
<b>H199</b>	7,8	8.1 ± 2	<b>4.5 ± 1.7</b>

pKa values predicted by PROPKA and the state of ionizable groups under different pH conditions are indicated. The protonation state of C29 at pH 8 were obtained taking into account deprotonation of H199 as previously proposed for papain. The protonation states of the catalytic residues (C29 and H199) are highlighted.

ionization of the catalytic C25 and H159 residues are coupled [29]. There the deprotonation of H159 shifts the pKa of C25 from ~3.3 to 7.6, while the neutralization of C25 decreases the pKa of H159 from ~8.5 to 4.3. Due to the direct relationship between catB and papain we assigned the protonation states of these residues according to this proposed mechanism.

The pKa values predicted with PROPKA thus appear to be sensitive to local microenvironment changes around the ionizable residues. In order to verify if the applied protonation profiles accurately represent the distinct pH conditions simulated, we collected 1000 snapshots (one at each 400 ps) from each molecular dynamics (MD) trajectory in order to perform pKa calculations. Table 1 shows the average pKa values during the MD simulations. From both pH conditions we obtained values consistent with the protonation states predicted from the crystal structure, thus confirming their validity. In this Table we have also highlighted the pKa shift in the catalytic residues C29 and H199 as observed for papain.

#### Electrostatic potential calculation and docking analyses reveal two heparin binding sites on catB structure

The electrostatic potential at the catB surface revealed the influence of the different protonation states for each of the pH conditions considered. Overall, independent of the conditions, the catB surface is mostly negative, presenting one region of positive potential in each domain (Fig. 2). Under alkaline conditions the overall surface is qualitatively more negative. The positive sites are composed of R85, K86, K130, K141 and K144 in the L-domain, and the catB N-terminus together with K154 and R235 in the R-domain. The protein's total charge changes from -11 at pH 8 to -5 at pH 5.5, with six key residues protonated exclusively under acidic conditions.

Experimental studies have provided knowledge about the affinity and kinetics of the catB-heparin interaction [22]. However, the precise binding site(s) has(have) not been defined. Taking into account that heparin-protein interactions are mainly driven by charge interactions due to the high number of sulfate groups found in the polysaccharide, we visually identified two regions of positive potential at the catB surface as potential heparin binding sites. Blind docking calculations confirmed this prediction, as we found two low energy clusters of docking poses coincident with these positive regions (Fig. 3A and B). Almeida and coworkers proposed that heparin mainly interacts with the occluding loop [22]. From a structural view this hypothesis appears unlikely due to the lack of charge and shape complementarity in this region of the enzyme, and is consistent with the absence of low-energy clusters for such a mode of binding in the docking results. Moreover, we carried out another

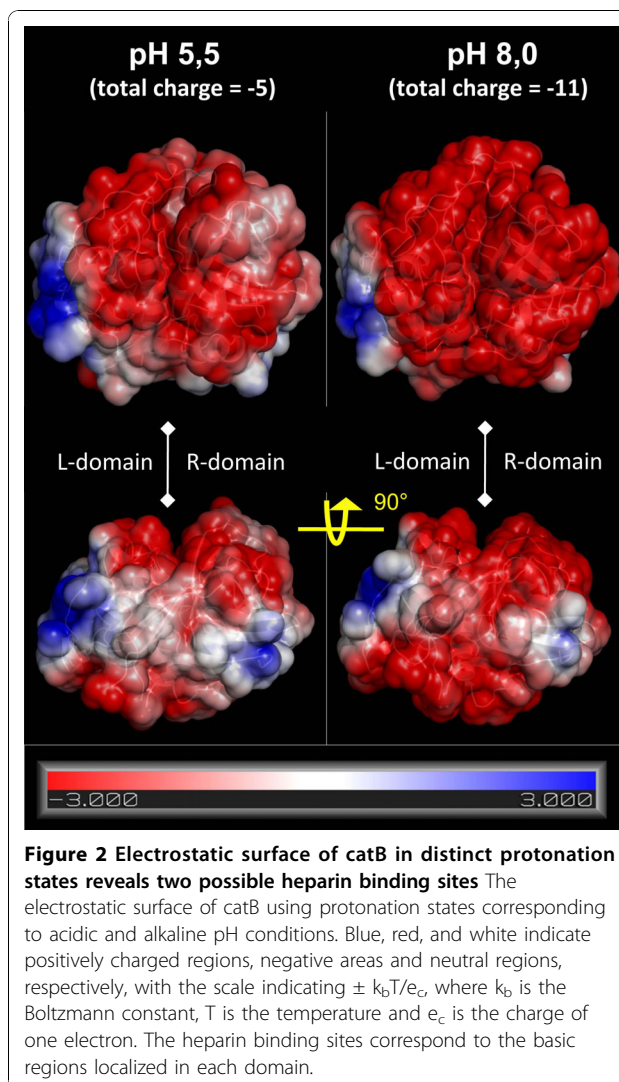
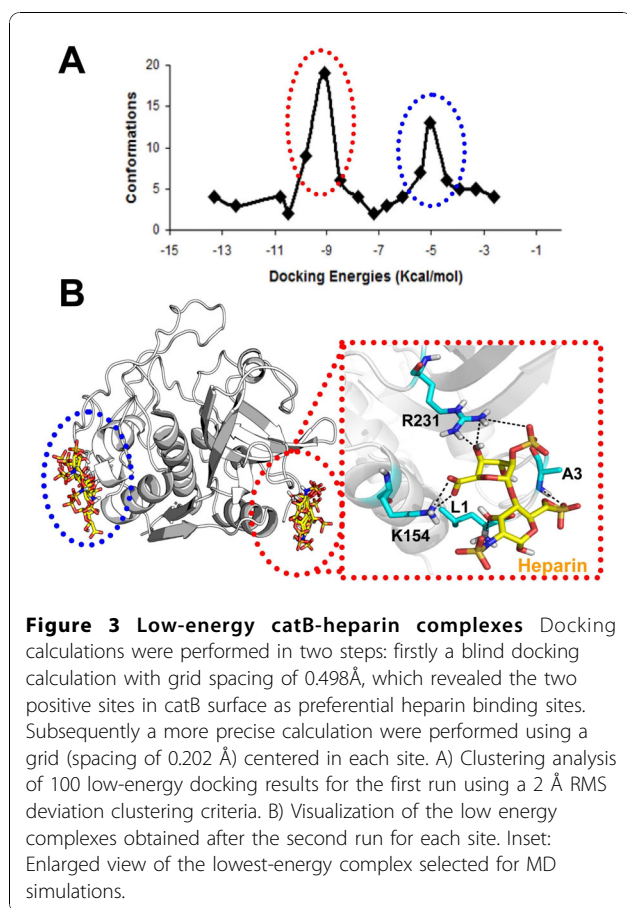


**Figure 2 Electrostatic surface of catB in distinct protonation states reveals two possible heparin binding sites** The electrostatic surface of catB using protonation states corresponding to acidic and alkaline pH conditions. Blue, red, and white indicate positively charged regions, negative areas and neutral regions, respectively, with the scale indicating  $\pm k_B T/e_c$ , where  $k_B$  is the Boltzmann constant, T is the temperature and  $e_c$  is the charge of one electron. The heparin binding sites correspond to the basic regions localized in each domain.

docking calculation verifying the atomic interactions in the heparin binding sites more precisely (see Methods). In the lowest energy complex obtained, heparin interacts with catB in the R-domain with an energy of -11 Kcal/mol (Fig. 3B). Although the positive potential at this site is smaller than that found in the L-domain, in R-domain site the van der Waals interactions were more favorable (contributed mainly by L1 at the N-terminus, A3, K154 and R231). We suggest that for a disaccharide the R-domain site is more important for this interaction; for longer sugar chains the L-domain could be also important for proper heparin accommodation.

#### catB protonation profile influences protein stability

As flexibility plays a key role in protein biological functions [30], we analyzed the root mean square fluctuation (RMSF) of catB backbone residues during MD for each condition simulated. A direct influence of protonation



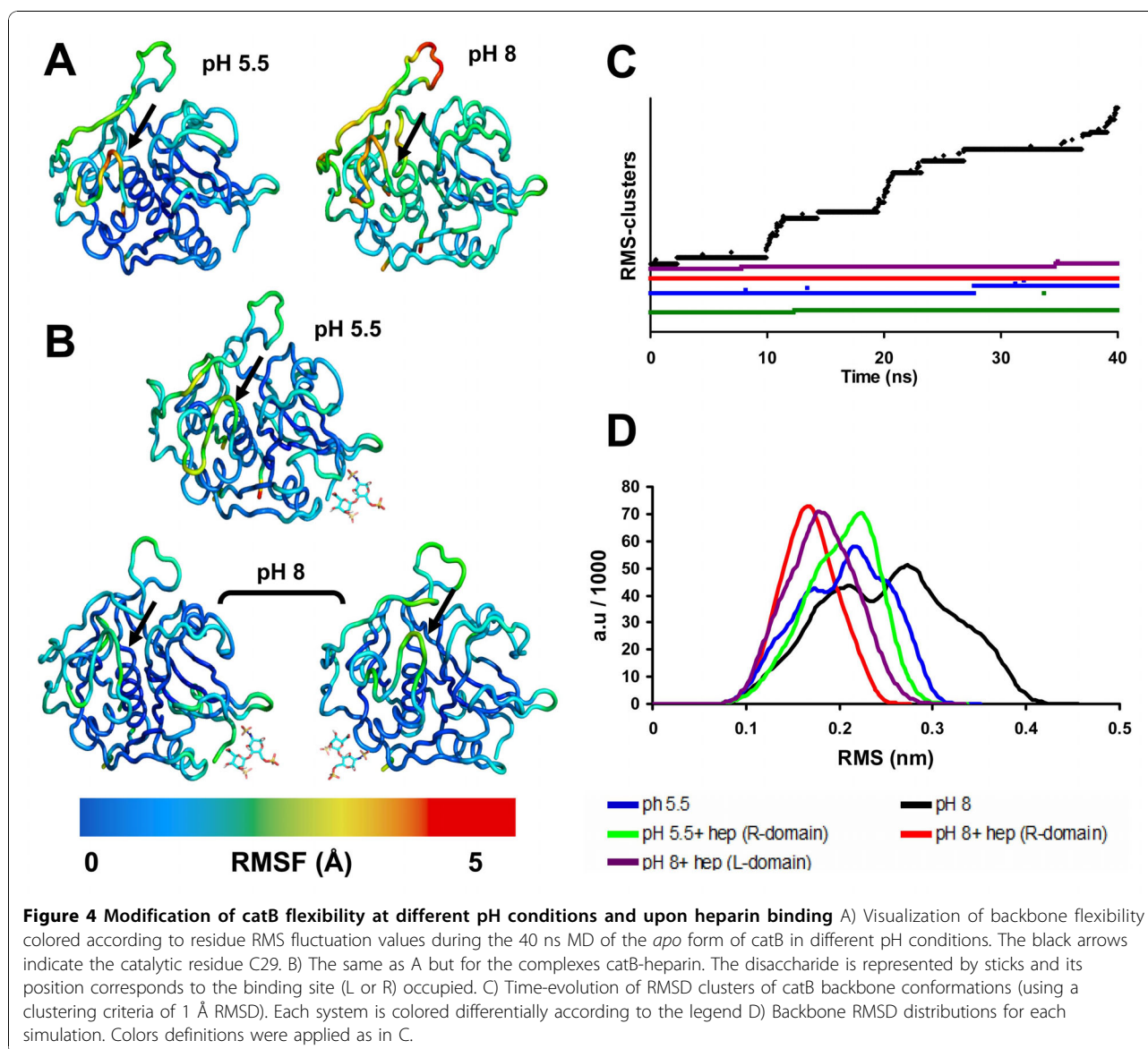
state on the overall enzyme flexibility is clearly seen. Figure 4A shows that at pH 5.5 the fluctuations were around 2Å, in contrast to RMSF values up to 5Å observed at pH 8.0. This behavior was reproducible: we performed replicate simulations (40 ns each) for each condition using different initial conditions (see Methods), with equivalent results (Additional file 1). In addition, we observed that functional regions such as the occluding loop and the active site presented the highest fluctuations at pH 8.0, revealing that alkaline conditions rapidly affected catB flexibility in regions directly involved with activity, independent of the starting structure (Fig. 4A and Additional file 1). Remarkably, this result shows that changes in protonation of a few residues can alter both local and non-local properties (hydrogen bonds, hydration layers and polar contacts). Local perturbations due to changes in protonation states have already been observed via MD simulations (e.g. [31]). However, in our simulations both local and global flexibility (large-scale protein motions) of catB were modified as a function of pH, corroborating experimental findings where catB loses its activity in alkaline pH in parallel with large structural changes [22].

### Heparin binding prevents catB destabilization in alkaline pH

In MD simulations of the bound enzyme at pH 5.5, the RMS fluctuation profile was seen to be similar to that of the apo form (Fig. 4B). Hence, catB is stable under acidic conditions independent of heparin binding. In contrast, under alkaline conditions heparin-bound catB exhibited much smaller backbone fluctuations (2 Å) than the very flexible apo form in these conditions. Moreover, we observed similar results when simulations were started using different initial conformations and also with heparin docked at the other binding site (L domain) (Fig. 4B). Functional regions including the occluding loop and the active site were also stabilized, showing that heparin binding at the predicted sites promotes a global stabilizing effect.

In Fig. 4C, we show the time-evolution of the number of distinct clusters of catB backbone conformations throughout the different MD simulations. Here each cluster contains conformations within an RMSD of 1 Å of the cluster center. If during a simulation the system visits numerous clusters, the RMSD from the starting structure will be very high, indicating conformational instability in the simulation. In contrast, if a simulation visits only a few (correspondingly larger) clusters, it can be considered as being more conformationally stable. Indeed, we found few clusters during the simulations of *apo* catB and the catB-heparin complex (4 and 2 clusters, respectively) under protonation conditions corresponding to pH 5.5 (Fig. 4C). Furthermore, in acidic conditions the backbone RMSD distributions, similar to the RMS fluctuation profiles, did not change significantly on binding heparin, presenting deviations in both cases centered at 2.2 Å. However, in the heparin-bound simulation in acidic conditions, the RMSD distribution began to shift towards a conformational state far from the native structure. (Fig. 4D).

Considering that catB loses stability and activity in alkaline conditions [22], in the systems simulated under protonation conditions corresponding to high pH we expected to observe a higher number of backbone clusters. This expectation was confirmed: we observed 66 clusters in the *apo* catB simulation (Fig. 4C). In addition, under these conditions the catB structure does not stabilize during the simulation, with a continuous increase of backbone RMSD values throughout the 40 ns production period. A similar profile was observed in the replica simulation and also when starting with another conformation (a separate PDB structure, see Methods), in which we found 47 clusters. The RMS fluctuations of both replica simulations, plus the simulation performed with the alternative catB structure (Additional file 1), showed similar results to the *apo* enzyme in alkaline conditions (Fig. 4A).

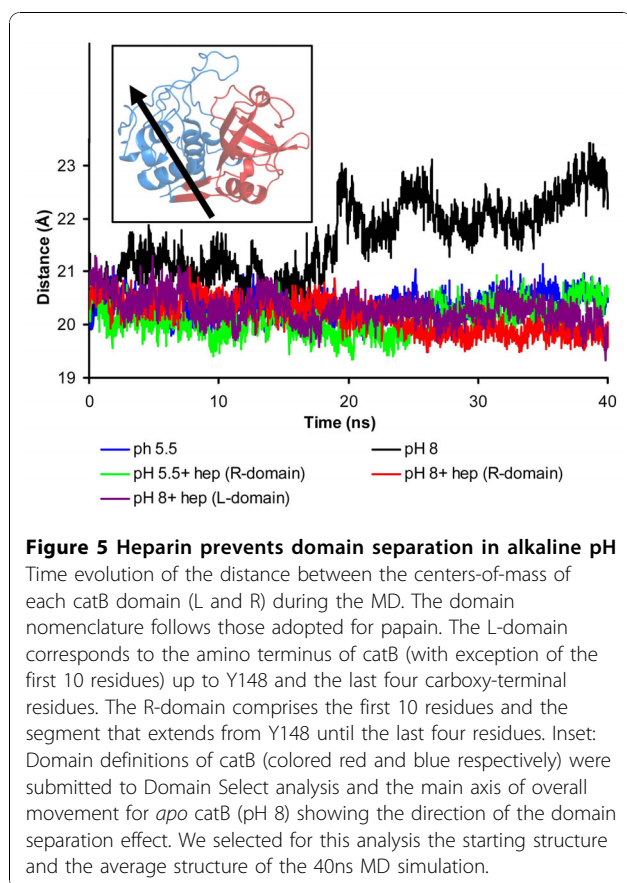


The RMSD distribution plot shows a clear shift dividing into two populations: one around 2 Å and the other at higher RMSD values. (Fig. 4D). On the other hand, in the simulation with heparin under alkaline conditions we observed fewer clusters comparable to acidic conditions (Fig. 4C). This stabilization afforded by heparin binding is also reflected in the RMSD distribution presenting a narrowed profile centered at small RMSD values (around 1.7 Å) (Fig. 4D).

#### Heparin prevents the domain separation observed in alkaline pH

It was previously postulated that the loss of inter-domain interface contacts should be a crucial event in catB inactivation in alkaline pH [32]. Furthermore, the

interface between L and R domains is essential not only for tertiary structure stabilization but also for the enzyme activity, as the catalytic triad is formed with residues from both domains [33]. To address whether this phenomenon is modulated by heparin, we compared the evolution of the distance between the centers of mass of the two domains during the simulations. In acidic conditions, this distance was stable at approximately 20 Å throughout the entire simulations, and was not significantly affected by heparin binding (Fig. 5). In contrast, when the enzyme was simulated under protonation conditions corresponding to alkaline medium, we observed a remarkable domain separation, with domain center-of-mass distances of up to 24 Å (Fig. 5). Further, we observed that this separation increased progressively



throughout the simulation, suggesting that total L and R domain separation could occur at longer time-scales. This certainly would affect catB catalysis, since the active site is found inserted into a V-shaped cleft between the L and R domains. A more detailed analysis provided by use of the DynDom software [34] revealed the separation of the L-domain as the principal overall motion of the enzyme in this condition, thus reinforcing this conclusion (Fig. 5). This domain motion was observed in all simulations except those containing heparin, in which it was not possible to identify large domain motions with the DynDom program. Remarkably, in these last systems, the interdomain distance remained at approximately 21 Å in alkaline conditions, comparable to acidic conditions. This shows that heparin binding governs the inter-domain stability even under unfavorable alkaline conditions and would presumably also allow the maintenance of protein activity.

#### Essential dynamics analysis reveals an allosteric role for heparin

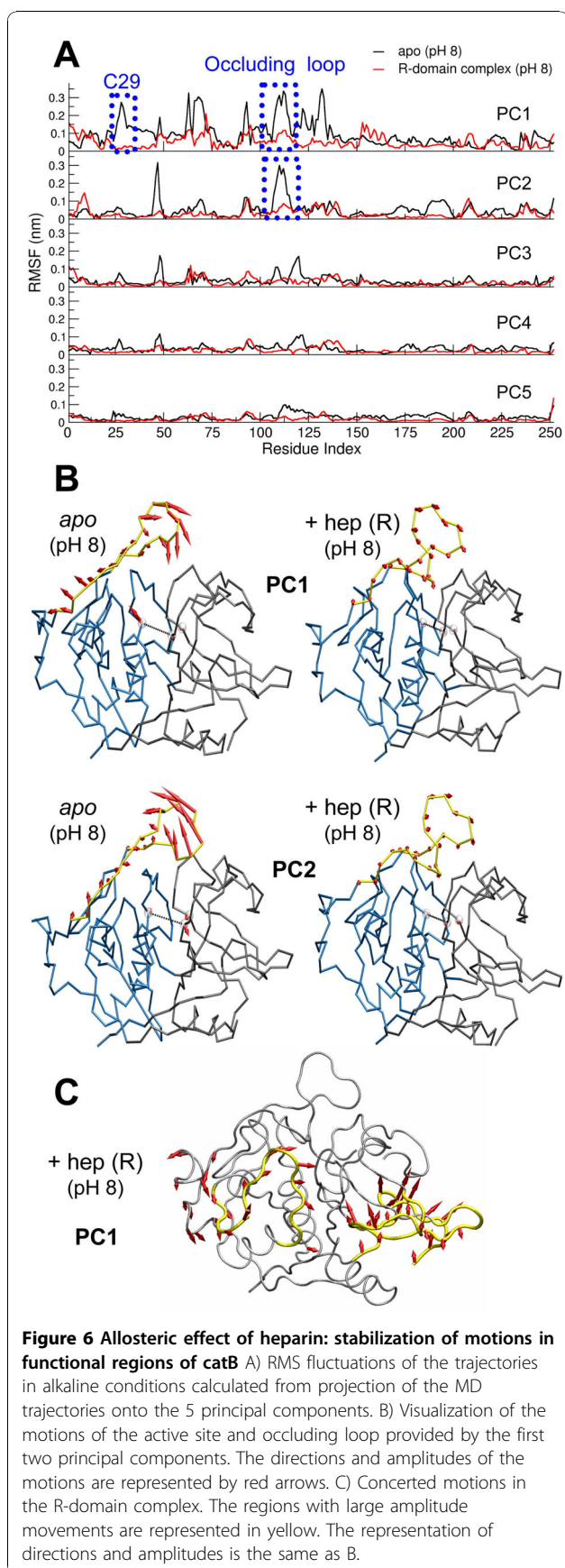
The results shown above suggest that catB as a whole and in particular the critical domain interface and occluding loop are stabilized by heparin binding to a relatively distant site in the R domain. From basic

thermodynamic principles, preferential binding of ligand to the native state will generally confer stability to a macromolecule in what has been described as an allosteric mechanism, without necessity for direct interaction between the ligand binding site and the active site residues, and has been extensively described in phenomenological terms [35]. The structural information available for catB, coupled with macromolecular simulations, provides a means for investigating details of such a mechanism directly.

We applied an essential dynamics analysis to examine the most relevant global macromolecular motions occurring during the simulations. Such analyses have been largely applied in the understanding of biological functions in proteins since they provide an evaluation of large-scale movements that are often related to domain motions and conformational changes [36]. We thus diagonalized the atomic positional covariance matrix to obtain the eigenvectors and corresponding eigenvalues. Selecting the first five (largest amplitude) principal components, we could recover around 60% of the total motions for *apo* catB and around 56% for heparin-bound catB. Our analysis focused on the systems simulated under alkaline conditions in order to address how heparin influences catB flexibility and prevents domain separation as shown above. We point out that certain analyses involving averaged quantities such as the essential dynamics and clustering approaches can be best interpreted for stable systems; the precise results for the *apo* catB under alkaline conditions will to some extent depend on the starting conformation. However, even under these conditions the overall results obtained were similar for replicated runs.

We examined the RMS fluctuations of each trajectory projected onto its five most representative principal components (PC). When comparing *apo* and complexed catB, we observed considerably lower fluctuations in the latter system for all PC analyzed (Fig. 6A). Further, we identified that the region around C29 and the occluding loop presented dramatically higher fluctuations in *apo* catB (reaching 3 Å in the two first PC), while in the complex these regions were shown to be very stable (deviations around 1 Å in all PC). The movements corresponding to the first two components were seen to comprise relevant motions of both the occluding loop and active site. Figure 6B shows the directions of individual residue movements and also their amplitudes, which are proportional to the lengths of the arrows in this representation.

By inspecting other motions corresponding to the first component (PC1) in the R-domain complexes, we identified local changes in the binding region. The residues close to the polysaccharide (L1, A3 K156 and R233) adopted a new conformation. To verify that these



motions would not lead to loss of binding interaction between catB and heparin, we measured the distance between the center of mass of heparin and the positive site during MD (Additional file 2) and found stable behavior: heparin remained bound during the entire simulation. Remarkably, however, this local motion is coupled to movements far from the heparin binding site. We observed that the residues 58 to 75 in the L-domain moved towards the interdomain interface (Fig. 6C). This motion certainly contributes to the stabilization of the overall structure, thus helping explain the results described above (Fig 4 and Fig 5). We did not find equivalent behavior in the L-domain complexes, which led us to investigate more deeply the correlated motions of catB in the *apo* form and in complex with heparin.

The analysis of cross correlation coefficients between pairs of residues is a useful method to identify correlated collective motions [37,38]. The correlation matrix represents the linear correlation between pairs of C-alpha atoms as they move about their average positions during dynamics. Positive correlations are related to motions occurring in the same direction whereas negative correlations indicate motion in opposite directions. We compared the correlation matrix of *apo* catB and of the complexes. In the *apo* form we observed positive intra-domain correlations but negative inter-domain correlations (Additional file 3). This pattern is not observed in the complexes, in which we identified a more diffuse pattern of correlations regardless of the binding site occupied. This result shows that heparin acts mainly as a stabilizing element, and its binding seems to restrict the anti-correlated collective motions that would be responsible for domain separation.

Concerning the occluding loop, we observed that the opening-closing movement is clearly represented by the two first components in *apo* catB. On the other hand, upon heparin binding these motions were not observed, independent of the binding site occupied. In addition, the first PC reveals the increasing distance between C29 and the other catalytic residues in *apo* catB, while in the complex this motion is absent. Therefore, heparin stabilizes catB motions in its functional regions. These results are consistent with experimental findings, which, although they revealed the implications of binding on the activity of the enzyme, did not provide a structural view of the phenomenon [22]. Heparin binding, despite the distance separating it from active site residues, prevents their disorganization as would otherwise be produced under alkaline conditions. The principal components obtained from the essential dynamics analysis of our MD simulations suggest that global concerted movements in the macromolecule leading to domain separation are suppressed by heparin binding, thus



helping explain an allosteric role for heparin in this biological system.

#### **Heparin prevents loss of helical content and stabilizes the occluding loop**

Loss of helical content was reported as the main effect related to alkaline-pH-induced inactivation of catB [22]. In the same study, it was reported that heparin prevented the loss of helical structure, which led to the postulate that the maintenance of activity in the catB-heparin complexes is strictly related to this structural aspect.

In analyzing the time evolution of secondary structural elements throughout the simulations, we observed stability of secondary structure elements in acidic conditions, independent of heparin binding (data not shown). In contrast, this same analysis for alkaline conditions revealed differences in the region of the main alpha helix (residues 28-45), which is located in the interdomain interface. Figure 7A shows the *phi-psi* distribution plot for the first residues of the main helix in alkaline conditions. It is clear that heparin binding maintained this region in helical form under alkaline conditions, whereas in the *apo* simulations the same region assumed a random coil profile. The fact that heparin was bound far from this helical region again emphasizes an allosteric mechanism for this stabilization. We also believe that the loss of helical content seen here on the 40 ns timescale is just a precursor of a major loss of secondary structure at longer timescales.

It is discussed in the literature that papain-like enzymes, which possess a similar domain organization, present structural characteristics that confer some rigidity to the active site region [29]. The most important element supporting this characteristic is the network of interactions in the interdomain interface. We verified the stability of the interaction between catalytic residues C29-H199 and found that disorganization of the main alpha helix in *apo* catB under alkaline conditions is coupled with the separation of the catalytic residues (Additional file 5). These events are strongly correlated with the overall domain motions observed. The binding of heparin at a substantial distance from the interface nevertheless stabilizes the interdomain contacts maintaining the structuring of the active site, and would explain the results obtained in biochemical assays [22].

The occluding loop controls access to the active site and also confers the *exo*-proteolytic activity of the enzyme. In our simulations, we verified the open-close mechanism of this region and found that in acidic conditions a stable closed state is maintained regardless of heparin binding. However, at pH 8.0 the occluding loop exhibited high flexibility in the absence of heparin (Fig. 7B) as expected after RMSF analysis (Fig 4A).

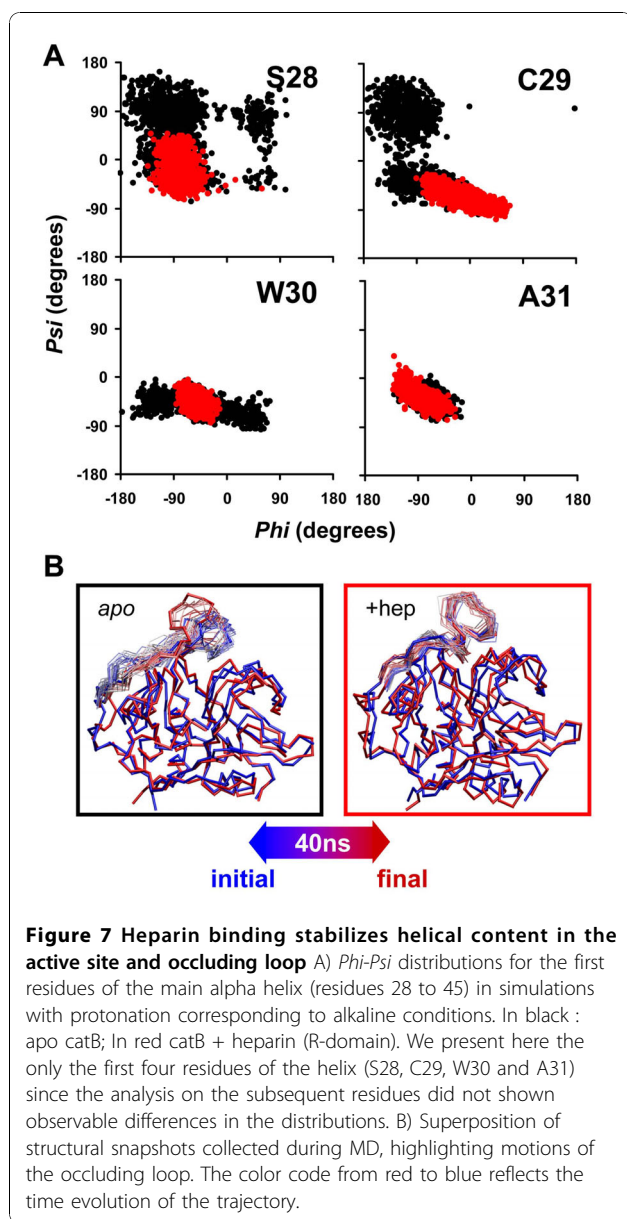
Nevertheless, under alkaline conditions, when heparin was bound the occluding loop exhibited a more stable conformation (Fig. 7B). In this conformation, besides closing the active site the occluding loop interacts with the R-domain in a distinct fashion from that observed in *apo* catB (Additional file 4). The occurrence of this conformation was also independent of the positive site occupied by heparin since the RMSD between the different complexes is around 1.4 Å. On the other hand, the loop conformations observed in the *apo* form simulations exhibit higher RMSD values (around 4.5 Å) compared to the complexes.

This result allows a discussion of experimental findings in which it was shown that heparin inhibits the *exo*-proteolytic activity of catB [22]. In that study, the authors proposed a competitive mechanism of inhibition due to the possible interaction of heparin with H110 and H111, which are the most important residues involved in accommodation of the negatively-charged C-terminal substrate carboxylate groups. From our analysis we conclude that the mechanism of inhibition promoted by heparin appears to be related also to the induction of conformational changes in catB, mainly in the occluding loop region, which adopts a distinct stable conformation that may impair proper binding of small substrates.

However, we cannot exclude the possibility that large heparin polymers may also bind to the occluding loop, thus inhibiting the *exo*-proteolytic activity of the enzyme, especially if the concentration of heparin increases as shown in ref. [22].

#### **A rearrangement of contacts explains heparin-induced stability at alkaline pH**

The catB interface is mainly polar and is stabilized by ion pairs and hydrogen bonds between buried residues [12]. Since we see that pH changes induce distinct protonation profiles mainly at the interface, and also that heparin binding affects the interface stability, we analyzed the atomic interactions in this region. In particular, we verified the permanency of interactions between interfacial residues in order to see the influence of heparin binding on their stability (Table 2). We first checked certain interactions suggested by experimental studies, such as W30- E171. This interaction was observed only in the acidic pH simulations (87% *apo* catB / 85% catB-hep), and does not occur in alkaline pH (see Fig. 1 and Table 1) due to deprotonation of the E171 carboxyl group which interacts with the backbone of W30. The protonation state of E171 also affects the interaction between this residue and W80, since the observed occupancies were higher in acidic pH (88% *apo* catB / 87% catB-hep) than in alkaline conditions (37% *apo* catB / 68% catB-hep). This interaction was suggested to be important in the overall maintenance of



the catB interface [12] and it was significantly stabilized by heparin binding. Other interactions found to be stabilized by heparin binding are detailed in Table 2.

An important aspect observed through the H-bonding analysis was the network of contacts between Q23, E36 and S220 (Fig. 8). Concerning the Q23 – S220 contact, we observed high stability in acidic pH. We identified two stable H-bonds between these residues in acidic simulations, while in alkaline conditions only one weak interaction was found. Further, the occupancy for each of these contacts was dependent on heparin binding, since their prevalence increasing from 65% to 82% in acidic conditions and 6% to 29% at higher pH. It appears that the lack of one H-bond between Q23 and

S220 in alkaline conditions is compensated by an interaction achieved between E36 and S220 only in such conditions. This occurs due to the distinctive protonation state of E36, which only when ionized (i.e., at pH 8) is able to interact with S220 through an H-bond. Remarkably, the occupancy of the E36-S220 interaction increases from 38% to 72% upon heparin binding. This result may be explained by the global stabilizing effect observed (see Essential dynamics analysis) which is crucial in the establishment of this distinct interdomain contact. The D22-H110 pair is another example of an interaction that was stabilized by the same mechanism. We measured the occupancy of this H-bonded state during the 40ns MD simulation. While in acidic pH conditions the occupancy of the hydrogen-bonded state was very high (80% apo catB / 79% catB-heparin), in alkaline conditions heparin binding significantly increased the stability of this interaction, which passed from 6% in *apo* catB to 67% in the catB-hep complex.

These results are correlated with the distinct loop conformation observed in the heparin bound complexes (Additional file 4). In addition, as shown, heparin binding at the R-domain induces a conformational change that leads to a more compact structure (Fig 6C). Further, heparin restricts collective motions involved in domain separation, which allows the stabilization of a distinct pattern of interactions formed in the interface under alkaline conditions.

## Conclusions

Heparin-protein interactions are known to regulate several biological processes including protease regulation [39], growth factor activity [40], macromolecular assembly [41] and viral mechanisms [42]. In this paper we unraveled the molecular mechanism of heparin protection against pH-induced inactivation of catB. This phenomenon was previously demonstrated through biochemical assays without a full understanding of the process because of the lack of structural information concerning heparin binding. Herein we were able to mimic the different pH conditions by performing MD simulations of catB with different protonation states according to pKa calculations. We confirmed experimental findings showing that under acidic conditions catB is stable. In contrast, at alkaline pH six residues are deprotonated, increasing the negative charge of the interdomain interface. This leads to charge repulsion and subsequent separation of the L and R domain. In addition, we observed the effect of the alkaline conditions in terms of destabilization of helical content, active-site disruption and increases in the flexibility of the occluding loop. All these events are closely related to loss of enzyme activity. Heparin binding counteracted these effects by a long-distance, allosteric mechanism

**Table 2 Occupancy of hydrogen bonds between interacting interface residues**

Interaction	Type	Percentage of occupancy of hydrogen bonds between interface residues			
		<i>apo</i> catB (pH 5,5)	<i>Apo</i> catB (pH 8,0)	catB + hep (pH 5,5)	catB + hep (pH 8,0)
W30 – E171	MC-SC	87%	—	85%	—
W80 – E171	SC-SC	88%	37%	87%	68%
D81 – S150	SC-SC	48%	6%	62%	55%
R41 – P169	SC-MC	70%	42%	83%	91%
Q23 – S220	MC-MC	65%	5%	82%	29%
	SC-SC	96%	—	90%	—
E36-S220	SC/SC	—	38%	—	72%
D22-H110	SC-SC	80%	6%	79%	67%

Interactions are broken down into main-chain (MC) and sidechain (SC). Domain definitions were used following papain domain organization.

which appears to be associated with (i) conformational changes leading to a more compact interface, and (ii) the restriction of catB flexibility, allowing stabilization and rearrangement of interdomain contacts under neutral/alkaline conditions. These new findings may be crucial for the design of new catB inhibitors.

## Methods

### Parameters for cathepsin B and heparin

The three-dimensional atomic coordinates of heparin were taken from the Protein Data Bank (entry 1HPN) [43]. From this structure we considered a heparin disaccharide for our studies. For docking and molecular dynamics we used the partial charges and force field parameters for heparin described in ref. [44]. The human cathepsin B crystal structure (PDB entry: 1HUC) [12] contains two proteins per asymmetric unit; the protein consisting of chains A and C was used as the starting structure for docking and MD simulations. The coordinates of catB complexed with CA-030 (PDB entry: 1CSB) [45] were also used to increase conformational sampling. We removed the coordinates of the inhibitor and the enzyme was treated as an *apo* form.

### pKa calculations

To obtain the pKa values for titratable catB residues we applied the PROPKA web server [26], using the catB crystal structure as input. This tool uses empirical parameters to estimate pKa values of each titratable residue in its chemical micro-environment, considering the contribution of H-bond formation, charge interactions and desolvation effects. This method was recently compared to other pKa predictive tools obtaining excellent results [46].

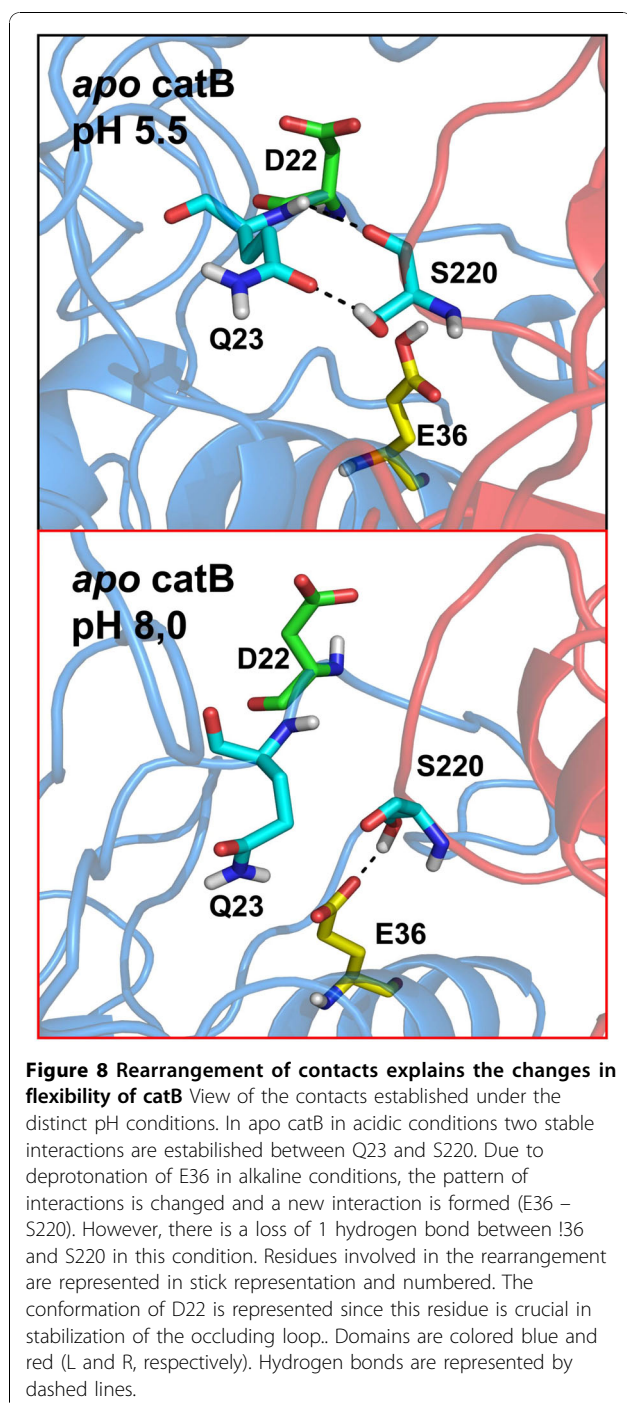
### Electrostatic surface analysis

With the results of the pKa analysis, we determine the most probable protonation state for each pH condition and added hydrogen atoms accordingly. Electrostatic

surface calculations were performed using APBS software [47]. This analysis combines the solvent accessible surface (SAS) calculation with the values of the electrostatic potential for each atom at the surface. This latter calculation is obtained by the resolution of the linearized Poisson-Boltzmann equation to obtain the surface charge distribution. Images were generated using PyMol [48].

### Molecular docking

The heparin disaccharide was docked as a ligand with free rotation for all its torsion angles (sulfate, hydroxyl groups and glycosidic bonds). Docking calculations were performed using the Lamarckian Genetic Algorithm (LGA) implemented in Autodock 3.0 [49], a program extensively used to predict proteins/polysaccharide binding modes [50]. We applied a two-step protocol. Initially we performed blind docking with a grid of probe-atom interaction energies and the electrostatic potential generated covering the whole protein with a spacing of 0.498 Å. This step was necessary to obtain the putative heparin binding sites on catB structure. Subsequently, we carried out runs taking into consideration only the regions around the most populated low energy clusters obtained from the blind docking. In this step we used a grid spacing of 0.202 Å to evaluate more precisely the atomic interactions in the binding sites. In all, we performed a total of 100 docking runs using a population of 200 individuals. The solutions within 2 Å root mean square deviation of each other were grouped in the same cluster, which were then ranked according to their docking energy values. We selected docked structures of heparin from the lowest energy clusters obtained in our calculations to assemble two distinct catB-heparin complexes, in which heparin was bound to either one or the other of the two catB domains. We identify these complexes according to the domain occupied by the sugar (L or R) and used these structures as starting points for the energy minimization / MD protocols.



#### Molecular dynamics simulation details

Molecular dynamics (MD) simulations, energy minimization and trajectory analyses were carried out with the GROMACS 3.1 package [51,52] using the GROMOS96 (G53a6) forcefield [53]. Different pH conditions were mimicked by changing the protonation states of six key residues accordingly to pKa calculations and experimental data as described above. Explicit SPC water

molecules [54] were used in all simulations, in which a 14 Å layer of water molecules were added around the solute molecules within a cubic water box, using periodic boundary conditions. Counter ions were inserted for system neutralization. LINCS [55] and SETTLE [56] were applied to constrain solute and solvent bonds, respectively. Temperature and pressure were kept at 310 K and 1 atm respectively by the Berendsen approach [57]. Electrostatic interactions were calculated with the PME method [58], using non-bonded cutoffs of 1.0 nm for Coulomb and 1.2 nm for van der Waals. The MD integration timestep was 2fs.

A three-step energy minimization protocol was used to avoid artifacts in atomic trajectories due to conversion of potential into kinetic energies: firstly, we applied the steepest-descent algorithm: *i*) 5000 steps with solute heavy atom positions restrained to their initial positions using a harmonic constant of 1 kJ/mol.nm in each Cartesian direction, allowing unrestrained water and hydrogen movement; and *ii*). 5000 steps with all atoms free to move. Subsequently, the conjugate-gradients algorithm was applied for further energy minimization until an energy gradient fell to 42 KJ/mol.nm. A preliminary MD (1 ns) with heavy atom positions restrained was performed to achieve solvent equilibration and system heating to 310 K. In this step, initial velocities were generated for each simulation. A replica simulation was performed for each system using different initial velocities. Then we performed a 3 ns unrestrained equilibration MD for each system followed by a 40ns production MD.

In the simulations of the heparin-bound complexes, we verified the heparin-catB interaction stability by measuring the time-evolution of the distances between the centers of masses of the heparin and catB positive domains (Additional file 2). This control is important to guarantee that the effects observed result from the maintenance of a stable complex during the entire simulation.

#### Essential dynamics analysis

We used the last 20 ns of the catB trajectories to obtain the covariance matrix of C-alpha atomic positions. In this step we applied the *g\_covar* module of GROMACS package. Rotation and translation motions were removed prior to covariance matrix calculation by least-squares superposition. All analyses were performed with the *g\_anaeig* module of GROMACS.

#### Cross correlation analysis

We projected the MD trajectory onto the first principal component, corresponding to the largest eigenvector, of the covariance matrix in order to visualize the extreme structures and the major fluctuations of the correlated

motions. The correlation matrix, a  $N \times N$  array whose  $i$ - $j$  entry  $Corr_{ij}$  summarizes the correlation between the motions of atoms  $i$  and  $j$ , is obtained from the reduction and normalization of the covariance matrix.

$$Corr_{ij} = \frac{\left\langle \left( \vec{r}_i - \vec{r}_{i,ave} \right) \cdot \left( \vec{r}_j - \vec{r}_{j,ave} \right) \right\rangle}{\sqrt{\left\langle \left( \vec{r}_i - \vec{r}_{i,ave} \right)^2 \right\rangle \left\langle \left( \vec{r}_j - \vec{r}_{j,ave} \right)^2 \right\rangle}}$$

### Domain motions analysis

Domain motions were analyzed with the Domain Select module of the DynDom software. This program compares two available structures of the same protein and deduces the rigid-body movement of one domain (the moving domain) relative to the other domain (the fixed domain) in the same way as the DynDom program. We selected the starting structure of each MD and the average structure of the respective simulation to be compared.

### Clustering analysis

We applied the `g_cluster` module of GROMACS package to calculate the RMS clusters of catB backbone conformations. Our clustering criteria was 1Å RMSD.

**Additional file 1: Similar RMS profiles of deviations are independent of the starting structure.** A) Visualization of backbone flexibility colored according to residue RMS fluctuation values during the 40 ns MD of the apo form of catB using the crystal structure with entry:1HUC . B) Same as A but using the crystal structure of catB entry 1CSB.

**Additional file 2: Heparin binding is stable throughout all the simulations** Mean values of the distances between the centers of mass of each binding site and heparin. Deviations are colored according to the binding site.

**Additional file 3: Cross correlation analysis of catB C-alpha atoms** A) Cross correlation matrix for the apo catB C-alpha atoms. B) Same as A but for the R-domain complex. C) Same as B but for the L-domain complex. Correlations close to 1 (colored in red) are related to motions in the same direction, whereas negative correlations are related to motions in opposite directions. In the upper left of each matrix are represented correlations with absolute values higher than 0.5. The domain organization of catB is represented close to each axis to clarify the interpretation of domain motions.

**Additional file 4: Heparin binding induces a distinct conformation of the occluding loop** Structural alignment of the average structures obtained from the MD simulations in alkaline conditions. Color definitions are represented. We represented the occluding loop region in tubes to highlight the distinct conformation adopted by this structural element when catB binds heparin.

**Additional File 5: Active site behavior during MD of apo catB at pH 5.5** Close-up view of the active-site region .The C-alpha of each catalytic residue (C29, H199 and N219) is represented as an orange sphere.

**Additional File 6: Active site behavior during MD of apo catB at pH 8.0** Close-up view of the active-site region .The C-alpha of each catalytic residue (C29, H199 and N219) is represented as an orange sphere.

**Additional File 7: Active site behavior during MD of catB-heparin complex at pH 5.5** Close-up view of the active-site region .The C-alpha

of each catalytic residue (C29, H199 and N219) is represented as an orange sphere.

**Additional File 8: Active site behavior during MD of catB-heparin complex at pH 8.0** Close-up view of the active-site region .The C-alpha of each catalytic residue (C29, H199 and N219) is represented as an orange sphere.

### Acknowledgements

We are grateful to MSc Roberta S Faccion for critical reading of the manuscript. We thank FAPERJ, CNPq and CAPES for financial support. This article has been published as part of *BMC Genomics* Volume 11 Supplement 5, 2010: Proceedings of the 5th International Conference of the Brazilian Association for Bioinformatics and Computational Biology. The full contents of the supplement are available online at <http://www.biomedcentral.com/1471-2164/11?issue=S5>.

### Author details

<sup>1</sup>Instituto de Biofísica Carlos Chagas Filho, Universidade Federal do Rio de Janeiro, 21949-901, Rio de Janeiro, Brasil. <sup>2</sup>Universidade de Mogi das Cruzes, 08780-911, Mogi das Cruzes, Brasil. <sup>3</sup>CNRS Laboratoire de Biochimie Théorique, Institut de Biologie Physico Chimique, 75005 Paris, France.

### Authors' contributions

MGSC designed the study, carried out all simulations and drafted the manuscript. PRB designed and coordinated the study, worked on data analysis and drafted the manuscript. CSS performed preliminary molecular docking and dynamics studies. CHR participated in interpreting the study and drafted the manuscript. PMB designed and coordinated the study. PGP designed and coordinated the study.

### Competing interests

The authors declare that they have no competing interests

Published: 22 December 2010

### References

1. Chapman HA, Riese RJ, Shi GP: **Emerging roles for cysteine proteases in human biology.** *Annual review of physiology* 1997, **59**:63-88.
2. Lutgens SP, Cleutjens KB, Daemen MJ, Heeneman S: **Cathepsin cysteine proteases in cardiovascular disease.** *Faseb J* 2007, **21**(12):3029-3041.
3. McKerrow JH: **Development of cysteine protease inhibitors as chemotherapy for parasitic diseases: insights on safety, target validation, and mechanism of action.** *International journal for parasitology* 1999, **29**(6):833-837.
4. Haque A, Banik NL, Ray SK: **New insights into the roles of endolysosomal cathepsins in the pathogenesis of Alzheimer's disease: cathepsin inhibitors as potential therapeutics.** *CNS & neurological disorders drug targets* 2008, **7**(3):270-277.
5. Martel-Pelletier J, Cloutier JM, Pelletier JP: **Cathepsin B and cysteine protease inhibitors in human osteoarthritis.** *J Orthop Res* 1990, **8**(3):336-344.
6. Gocheva V, Joyce JA: **Cysteine cathepsins and the cutting edge of cancer invasion.** In *Cell cycle. Volume 6*. Georgetown, Tex; 2007:(1):60-64.
7. Jedeszko C, Sloane BF: **Cysteine cathepsins in human cancer.** *Biological chemistry* 2004, **385**(11):1017-1027.
8. Joyce JA, Hanahan D: **Multiple roles for cysteine cathepsins in cancer.** In *Cell cycle. Volume 3*. Georgetown, Tex; 2004:(12):1516-1619.
9. Kostoulas G, Lang A, Nagase H, Baiçi A: **Stimulation of angiogenesis through cathepsin B inactivation of the tissue inhibitors of matrix metalloproteinases.** *FEBS letters* 1999, **455**(3):286-290.
10. Palermo C, Joyce JA: **Cysteine cathepsin proteases as pharmacological targets in cancer.** *Trends in pharmacological sciences* 2008, **29**(1):22-28.
11. Krupa JC, Hasnain S, Nagler DK, Menard R, Mort JS: **S2' substrate specificity and the role of His110 and His111 in the exopeptidase activity of human cathepsin B.** *The Biochemical journal* 2002, **361**(Pt 3):613-619.
12. Musil D, Zucic D, Turk D, Engh RA, Mayr I, Huber R, Popovic T, Turk V, Towatari T, Katunuma N, et al: **The refined 2.15 Å X-ray crystal structure of human liver cathepsin B: the structural basis for its specificity.** *The EMBO journal* 1991, **10**(9):2321-2330.

13. Illy C, Quraishi O, Wang J, Purisima E, Vernet T, Mort JS: **Role of the occluding loop in cathepsin B activity.** *The Journal of biological chemistry* 1997, **272**(2):1197-1202.
14. Nagler DK, Storer AC, Portaro FC, Carmona E, Juliano L, Menard R: **Major increase in endopeptidase activity of human cathepsin B upon removal of occluding loop contacts.** *Biochemistry* 1997, **36**(41):12608-12615.
15. Frlan R, Gobec S: **Inhibitors of cathepsin B.** *Current medicinal chemistry* 2006, **13**(19):2309-2327.
16. Cathers BE, Barrett C, Palmer JT, Ryzdzewski RM: **pH Dependence of inhibitors targeting the occluding loop of cathepsin B.** *Bioorganic chemistry* 2002, **30**(4):264-275.
17. Cavallo-Medved D, Rudy D, Blum G, Bogoy M, Caglic D, Sloane BF: **Live-cell imaging demonstrates extracellular matrix degradation in association with active cathepsin B in caveolae of endothelial cells during tube formation.** *Experimental cell research* 2009, **315**(7):1234-1246.
18. Cavallo-Medved D, Sloane BF: **Cell-surface cathepsin B: understanding its functional significance.** *Current topics in developmental biology* 2003, **54**:313-341.
19. Mohamed MM, Sloane BF: **Cysteine cathepsins: multifunctional enzymes in cancer.** *Nature reviews* 2006, **6**(10):764-775.
20. Sloane BF, Rozhin J, Lah TT, Day NA, Buck M, Ryan RE, Crissman JD, Honn KV: **Tumor cathepsin B and its endogenous inhibitors in metastasis.** *Advances in experimental medicine and biology* 1988, **233**:259-268.
21. Coombe DR, Kett WC: **Heparan sulfate-protein interactions: therapeutic potential through structure-function insights.** *Cell Mol Life Sci* 2005, **62**(4):410-424.
22. Almeida PC, Nantes IL, Chagas JR, Rizzi CC, Faljoni-Alario A, Carmona E, Juliano L, Nader HB, Tersariol IL: **Cathepsin B activity regulation. Heparin-like glycosaminoglycans protect human cathepsin B from alkaline pH-induced inactivation.** *The Journal of biological chemistry* 2001, **276**(2):944-951.
23. Almeida PC, Nantes IL, Rizzi CC, Judice WA, Chagas JR, Juliano L, Nader HB, Tersariol IL: **Cysteine proteinase activity regulation. A possible role of heparin and heparin-like glycosaminoglycans.** *The Journal of biological chemistry* 1999, **274**(43):30433-30438.
24. Lim IT, Meroueh SO, Lee M, Heeg MJ, Mobashery S: **Strategy in inhibition of cathepsin B, a target in tumor invasion and metastasis.** *Journal of the American Chemical Society* 2004, **126**(33):10271-10277.
25. Zhou Z, Wang Y, Bryant SH: **Computational analysis of the cathepsin B inhibitors activities through LR-MMPBSA binding affinity calculation based on docked complex.** *Journal of computational chemistry* 2009.
26. Li H, Robertson AD, Jensen JH: **Very fast empirical prediction and rationalization of protein pKa values.** *Proteins* 2005, **61**(4):704-721.
27. Harris TK, Turner GJ: **Structural basis of perturbed pKa values of catalytic groups in enzyme active sites.** *IUBMB life* 2002, **53**(2):85-98.
28. Pinitglang S, Watts AB, Patel M, Reid JD, Noble MA, Gul S, Bokth A, Naeem A, Patel H, Thomas EW, et al: **A classical enzyme active center motif lacks catalytic competence until modulated electrostatically.** *Biochemistry* 1997, **36**(33):9968-9982.
29. Dardenne LE, Werneck AS, de Oliveira Neto M, Bisch PM: **Electrostatic properties in the catalytic site of papain: A possible regulatory mechanism for the reactivity of the ion pair.** *Proteins* 2003, **52**(2):236-253.
30. Huber R, Bennett WS Jr: **Functional significance of flexibility in proteins.** *Biopolymers* 1983, **22**(1):261-279.
31. Varma S, Chiu SW, Jakobsson E: **The influence of amino acid protonation states on molecular dynamics simulations of the bacterial porin OmpF.** *Biophysical journal* 2006, **90**(1):112-123.
32. Turk B, Dolenc I, Zerovnik E, Turk D, Gubensek F, Turk V: **Human cathepsin B is a metastable enzyme stabilized by specific ionic interactions associated with the active site.** *Biochemistry* 1994, **33**(49):14800-14806.
33. Turk B, Turk V, Turk D: **Structural and functional aspects of papain-like cysteine proteinases and their protein inhibitors.** *Biological chemistry* 1997, **378**(3-4):141-150.
34. Hayward S, Berendsen HJ: **Systematic analysis of domain motions in proteins from conformational change: new results on citrate synthase and T4 lysozyme.** *Proteins* 1998, **30**(2):144-154.
35. Robert CH, Colosimo A, Gill SJ: **Allosteric formulation of thermal transitions in macromolecules, including effects of ligand binding and oligomerization.** *Biopolymers* 1989, **28**(10):1705-1729.
36. Berendsen HJ, Hayward S: **Collective protein dynamics in relation to function.** *Current opinion in structural biology* 2000, **10**(2):165-169.
37. de Oliveira CAF, Guimaraes CRW, Barreiro G, de Alencastro RB: **Human cytomegalovirus protease: Why is the dimer required for catalytic activity?** *Journal of Chemical Theory and Computation* 2007, **3**(1):278-288.
38. Hunenberger PH, Mark AE, Vangunsteren WF: **Fluctuation and Cross-Correlation Analysis of Protein Motions Observed in Nanosecond Molecular-Dynamics Simulations.** *Journal of molecular biology* 1995, **252**(4):492-503.
39. Jin L, Abrahams JP, Skinner R, Petitou M, Pike RN, Carrell RW: **The anticoagulant activation of antithrombin by heparin.** *Proceedings of the National Academy of Sciences of the United States of America* 1997, **94**(26):14683-14688.
40. Mach H, Volkin DB, Burke CJ, Middaugh CR, Linhardt RJ, Fromm JR, Loganathan D, Mattsson L: **Nature of the interaction of heparin with acidic fibroblast growth factor.** *Biochemistry* 1993, **32**(20):5480-5489.
41. Chen Y, Maguire T, Hileman RE, Fromm JR, Esko JD, Linhardt RJ, Marks RM: **Dengue virus infectivity depends on envelope protein binding to target cell heparan sulfate.** *Nature medicine* 1997, **3**(8):866-871.
42. Harrop HA, Coombe DR, Rider CC: **Heparin specifically inhibits binding of V3 loop antibodies to HIV-1 gp120, an effect potentiated by CD4 binding.** In *AIDS. Volume 8.* London, England; 1994:(2):183-192.
43. Mulloy B, Forster MJ, Jones C, Davies DB: **N.m.r. and molecular-modelling studies of the solution conformation of heparin.** *The Biochemical journal* 1993, **293**(Pt 3):849-858.
44. Verli H, Guimaraes JA: **Molecular dynamics simulation of a decasaccharide fragment of heparin in aqueous solution.** *Carbohydrate research* 2004, **339**(2):281-290.
45. Turk D, Podobnik M, Popovic T, Katunuma N, Bode W, Huber R, Turk V: **Crystal structure of cathepsin B inhibited with CA030 at 2.0-A resolution: A basis for the design of specific epoxysuccinyl inhibitors.** *Biochemistry* 1995, **34**(14):4791-4797.
46. Davies MN, Toseland CP, Moss DS, Flower DR: **Benchmarking pK(a) prediction.** *BMC biochemistry* 2006, **7**:18.
47. Baker NA, Sept D, Joseph S, Holst MJ, McCammon JA: **Electrostatics of nanosystems: application to microtubules and the ribosome.** *Proceedings of the National Academy of Sciences of the United States of America* 2001, **98**(18):10037-10041.
48. Delano WL: **The PyMOL Molecular Graphics System.** 1998.
49. Morris GM, Goodsell DS, Halliday RS, Huey R, Hart WE, Belew RK, Olson AJ: **Automated docking using a Lamarckian genetic algorithm and an empirical binding free energy function.** *Journal of computational chemistry* 1998, **19**(14):1639-1662.
50. Bitomsky W, Wade RC: **Docking of Glycosaminoglycans to Heparin-Binding Proteins: Validation for aFGF, bFGF, and Antithrombin and Application to IL-8.** *Journal of the American Chemical Society* 1999, **121**(13):3004-3013.
51. Hess B, Kutzner C, Van Der Spoel D, Lindahl E: **GROMACS 4: Algorithms for Highly Efficient, Load-Balanced, and Scalable Molecular Simulation.** *Journal of chemical theory and computation* 2008, **4**(2):435.
52. Van der Spoel D, Lindahl E, Hess B, van Buuren AR, Apol E, Meulenhoff PJ, Tieleman DP, Sijbers aLTM, Feenstra KA, van Drunen R, Berendsen H.J.C.: **Gromacs User Manual version 3.2.** 2004.
53. Oostenbrink C, Villa A, Mark AE, van Gunsteren WF: **A biomolecular force field based on the free enthalpy of hydration and solvation: the GROMOS force-field parameter sets 53A5 and 53A6.** *Journal of computational chemistry* 2004, **25**(13):1656-1676.
54. Berendsen HJC PJ, Van Gunsteren WF, Hermans J: **"Intermolecular Forces".** 1981.
55. Hess B, Bekker H, Berendsen HJC, Fraaije JGEM: **LINCS: A linear constraint solver for molecular simulations.** *Journal of computational chemistry* 1997, **18**:1463-1472.
56. Miyamoto S, Kollman PA: **Settle - an Analytical Version of the Shake and Rattle Algorithm for Rigid Water Models.** *Journal of computational chemistry* 1992, **13**:952-962.

57. Berendsen HJC, Postma JPM, Vangunsteren WF, Dinola A, Haak JR: **Molecular-Dynamics with Coupling to an External Bath.** *J Chem Phys* 1984, **81**:3684-3690.
58. Ulrich E, Lalith P, Max LB, Tom D, Hsing L, Lee GP: **A smooth particle mesh Ewald method.** *J Chem Phys* 1995, **103**:8577-8593.

doi:10.1186/1471-2164-11-S5-S5

**Cite this article as:** Costa *et al.*: How does heparin prevent the pH inactivation of cathepsin B? Allosteric mechanism elucidated by docking and molecular dynamics. *BMC Genomics* 2010 **11**(Suppl 5):S5.

**Submit your next manuscript to BioMed Central  
and take full advantage of:**

- Convenient online submission
- Thorough peer review
- No space constraints or color figure charges
- Immediate publication on acceptance
- Inclusion in PubMed, CAS, Scopus and Google Scholar
- Research which is freely available for redistribution

Submit your manuscript at  
[www.biomedcentral.com/submit](http://www.biomedcentral.com/submit)

